Photochemical & Photobiological Sciences (2022) 21:1845–1852
https://doi.org/10.1007/s43630-022-00261-9

ORIGINAL PAPERS

Analysis of molecular photomechanical performance using a one-dimensional harmonic model

Adam J. Berges[1] · **Christopher J. Bardeen**[1]

Received: 24 April 2022 / Accepted: 27 June 2022 / Published online: 24 July 2022

Abstract

The photochemical reaction of a molecule leads to a change in the position of its nuclei that can be harnessed to perform mechanical work. Photomechanical materials use this effect to act as light-powered actuators. In this paper, a one-dimensional model based on coupled harmonic potential energy surfaces is developed to describe the photomechanical response of a molecule. This model generates predictions that are qualitatively consistent with standard mechanochemistry models for ground state rate reactions. To analyze the photomechanical process, excited state dynamics like photon absorption and relaxation are included. The model allows us to derive analytical expressions for the work output, blocking force, and absorbed photon-to-work efficiency. The effects of nonadiabatic electronic coupling, unequal frequency potentials, and the cycling efficiency are also analyzed. If the starting state is the stable (lower energy) isomer, it is possible to attain photon-to-work efficiencies up to 55.4%. If initial state is higher in energy, for example a metastable isomer, then one-way efficiencies > 100% are possible due to the release of stored potential energy. Photomechanical materials can be competitive with photovoltaic–piezoelectric combinations in terms of efficiency, but current materials will require substantial improvement before they can approach the theoretical limits.

Graphical abstract

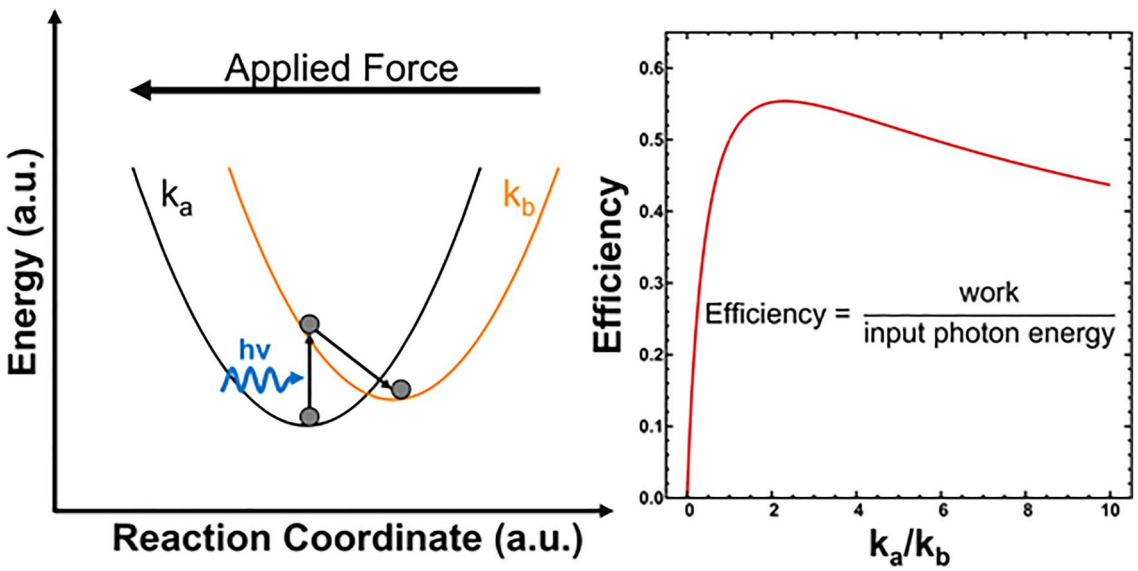

✉ Christopher J. Bardeen
christopher.bardeen@ucr.edu

[1] Department of Chemistry, University of California, Riverside, Riverside, CA 92521, USA

1 Introduction

The use of photons to transport energy is appealing thanks to their ability to propagate long distances with low loss, their resistance to electromagnetic interference, and their wide range of controllable parameters like wavelength, polarization, and coherence. Once they reach their destination, however, photons must be converted to a more useful form of energy, like heat or mechanical work. To generate mechanical work, one option is to convert them into an electrical potential that can be harnessed to drive actuator devices. This strategy requires two elements: a photovoltaic module to generate current, and a device to convert this electrical energy into a mechanical output, like an electric motor or piezoelectric crystal. Another option is to utilize a material that directly converts the absorbed photon into mechanical motion without relying on free electrons and external circuitry. Photomechanical materials have the property that their constituent nuclei change position after photon absorption, generating a force and displacement that can be harnessed to perform mechanical work [1–3]. This change in atomic coordinates could result from heating (photothermal) [4–6], a change in electronic state (photostrictive) [7], or a chemical reaction (photochemical) [8].

The photochemical approach to photomechanical materials relies on harnessing molecular reactions, like cis–trans isomerization, to drive deformations in solid-state systems like polymers [9–11] and crystals [12–17]. To be useful in practical actuator devices, the photochemical product should be able to return to the reactant state either by thermal fluctuations (T-type reversibility) or by a second photon absorption (P-type reversibility) [18, 19]. To assess the potential of this class of photomechanical materials, specifically their efficiency and work output, it would be useful to have a simple theoretical framework that could be used to analyze such systems at the molecular level. The Bell model for mechanochemistry [20] and the Marcus–Hush model for electron transfer [21] are examples of semiclassical approaches based on displaced harmonic oscillators. An analogous model for the photomechanical response of a molecule could provide the basis for interpretation of experimental results and the design of improved materials. Such a framework could also help address practical questions, like how the photomechanical approach to energy conversion compares to the photovoltaic approach in terms of figures of merit like efficiency.

The goal of this paper is to develop a simple one-dimensional (1D) model that can serve as a starting point for more realistic models of the photomechanical response. First, we introduce the harmonic model with two states, denoted $|a\rangle$ and $|b\rangle$, that correspond to two different nuclear configurations. When an external force is applied, this simple model generates predictions that are qualitatively consistent with standard mechanochemistry models. We next analyze the photomechanical process and derive expressions for the work output, blocking force, and absorbed photon-to-work efficiency of the $|a\rangle \rightarrow |b\rangle$ reaction. If the starting state $|a\rangle$ is the stable isomer (lower energy than $|b\rangle$), we find that it is possible to attain photon-to-work efficiencies of $> 50\%$. If $|a\rangle$ is higher in energy, i.e., a metastable isomer, then one-way efficiencies $> 100\%$ are possible by releasing the stored potential energy. We also analyze the effects of nonadiabatic electronic coupling, unequal frequency potentials, and the $|a\rangle \rightarrow |b\rangle \rightarrow |a\rangle$ cycling efficiency. We conclude that photomechanical materials have the potential to surpass a photovoltaic-piezoelectric combination and approach that of a photovoltaic–motor combination. Given that most measured photomechanical efficiencies are orders of magnitude below the theoretical limits derived in this paper, our results suggest that there is substantial room for improvement in this class of materials.

2 Results

The model used for our calculations is shown in Fig. 1 [22]. Two harmonic potential energy surfaces represent electronic states $|a\rangle$ and $|b\rangle$. We always assume the system starts in state $|a\rangle$. The force constants are k_a and k_b, respectively, and the coordinate system is chosen, so that the minima lie at $\pm x_0$

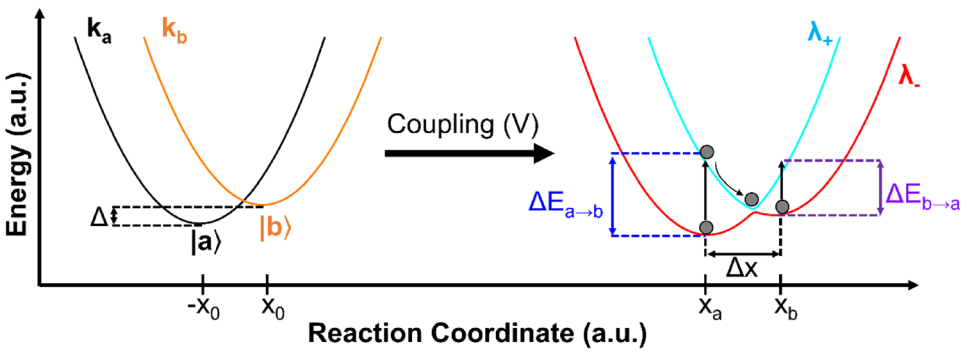

Fig. 1 **a** Two uncoupled diabatic harmonic surfaces, centered at $\pm x_0$, with energy offset Δ, that serve as the starting point for the calculations. **b** Adiabatic $\lambda_{\pm}$ energy surfaces created by electronic coupling term V, along with the relevant energy gaps

along the reaction coordinate in the absence of an applied force. State $|b\rangle$ is offset in energy by an amount Δ. If Δ is positive, then the initial state $|a\rangle$ is the lowest energy, stable state and state $|b\rangle$ can be associated with either a relaxed excited state or an isomerized molecule. If $\Delta < 0$, then state $|a\rangle$ is a higher energy, metastable state that must be populated by some other process, e.g., previous absorption of a photon. Finally, states $|a\rangle$ and $|b\rangle$ are coupled by an interaction term V, which we assume to be a real number. The overall Hamiltonian is given by

$$\hat{H} = |a\rangle E_a \langle a| + |b\rangle E_b \langle b| + V(|a\rangle\langle b| + |b\rangle\langle a|) \quad (1)$$

with

$$E_a = \frac{1}{2}k_a\left(x + x_0\right)^2, \quad (2a)$$

$$E_b = \frac{1}{2}k_b\left(x - x_0\right)^2 + \Delta. \quad (2b)$$

Diagonalization of this Hamiltonian generates two adiabatic potential energy surfaces (PESs) whose energies $\lambda_{\pm}$ are given by

$$\lambda_{\pm}(x) = \frac{1}{2}\left[E_a(x) + E_b(x) \pm \sqrt{\left(E_b(x) - E_a(x)\right)^2 + 4V^2}\right]. \quad (3)$$

If a constant force A is applied that pushes the system to the left in Fig. 1a, i.e., toward state $|a\rangle$, we have an additional potential energy term $U(x) = -Ax$. This force resists the $|a\rangle \rightarrow |b\rangle$ reaction and modifies the Hamiltonian. If we neglect V, the new $|a\rangle$ and $|b\rangle$ PES curves are given by

$$E_a(x) = \frac{1}{2}k_a\left(x - \left(-x_0 - \frac{A}{k_a}\right)\right)^2 + Ax_a - \frac{A^2}{2k_a}, \quad (4a)$$

$$E_b(x) = \frac{1}{2}k_b\left(x - \left(+x_0 - \frac{A}{k_b}\right)\right)^2 + Ax_b - \frac{A^2}{2k_b} + \Delta. \quad (4b)$$

The modified PESs are shown in Fig. 1b. The applied force shifts the potential minima to new positions x_a and x_b. The barrier height between the new $|a\rangle$ and $|b\rangle$ minima (x_a and x_b) is lowered by the force and disappears when the potential curve of $|a\rangle$ crosses through the minimum of the $|b\rangle$ potential well, as shown in Fig. 2a. The force at which the potential minimum at x_b disappears is denoted the blocking force or stop force A_{stop} and represents the maximum force under which the system can maintain two stable points. Note that as A increases, the optical gaps between the $|a\rangle$ and $|b\rangle$ surfaces at stable points x_a and x_b also change, with the gap at x_a increasing and that at x_b decreasing (Fig. 2b).

At this point, it is useful to place this model in the context of mechanochemical systems, where the reaction rate depends on the ground state energy barrier between x_b and x_a [23]. If we assume that $|b\rangle$ is the reactant that must reach the lower energy product state $|a\rangle$, we can calculate the barrier as a function of A for various parameter values. Figure 3 plots the barrier height $\Delta E^{\ddagger}$ versus A for various nonadiabatic coupling values V. For low A values, there is a linear dependence of $\Delta E^{\ddagger}$ on A, which saturates at larger forces. This linear dependence of $\Delta E^{\ddagger}$ on A is consistent with most theoretical treatments of the effects of an applied force on reaction rates [24, 25]. Note that the net effect is to change the thermal $|b\rangle \rightarrow |a\rangle$ rate. No thermodynamic work is performed, since the motion along the reaction coordinate is parallel to the applied force.

We now turn to the photomechanical process in which the system is forced to work against the applied force by photoexcitation from $|a\rangle$ to $|b\rangle$. The system starts at x_a, absorbs a photon to go to the upper surface, and relaxes to x_b, as shown in Fig. 1b. The work output W in this case is given by the usual definition of force × distance

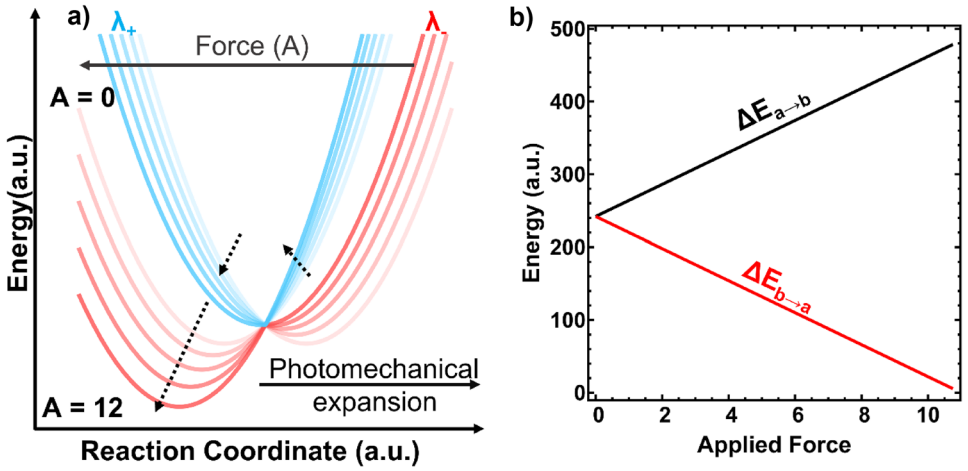

Fig. 2 **a** As the force acting against photoisomerization increases, both the ground state (λ_-) and excited state (λ_+) energy minima shift to the left. Eventually, the barrier between the ground state minima vanishes. **b** The shifts in the optical gaps (ΔE) as a function of applied force A. For these calculations, $x_0 = 11$, $k_a = k_b = 1$, $A_{stop} = 11$

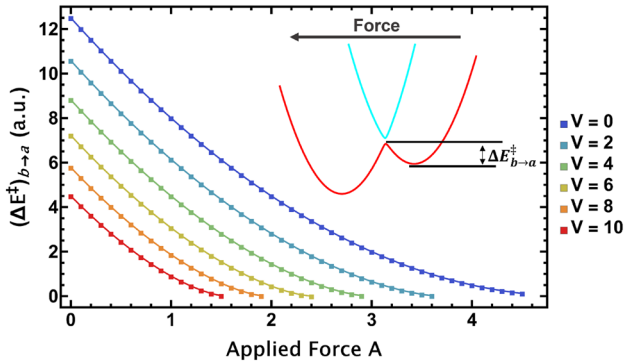

Fig. 3 The dependence of the ground state activation energy $\Delta E^{\ddagger}_{b\to a}$ as the applied force A is increased for different values of the electronic coupling V. For these calculations, $k_a = k_b = 1$, $x_0 = -5$, and $\Delta = 0$. Inset: illustration of the ground state PES (red) showing $\Delta E^{\ddagger}_{b\to a}$

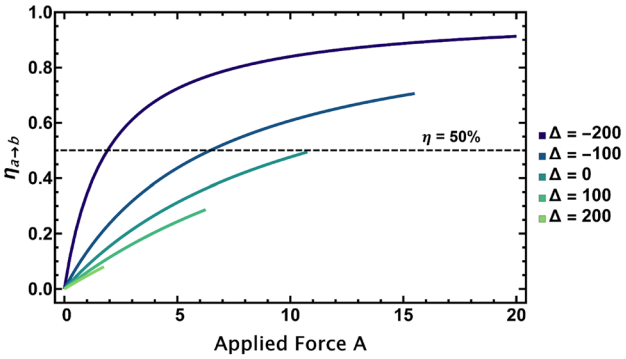

Fig. 4 The photomechanical efficiency $\eta_{a\to b}$ plotted as a function of applied force A and different Δ energy offsets. These calculations were done with $x_0 = 11$, $k_a = k_b = 1$, and $V = 0$. For these parameters, the maximum efficiency occurs at A_{stop} for all these Δ values

$$W_{a\to b} = A\left(x_b - x_a\right) = A\Delta x. \tag{5}$$

The input photon energy is just the difference between the $|a\rangle$ and $|b\rangle$ potentials at the starting position x_a:

$$\Delta E_{a\to b} = E_b\left(x_a\right) - E_a\left(x_a\right). \tag{6}$$

With V = 0, we can use Eqs. (4–6) to find

$$E_{a\to b} = 2k_b x_0^2 + 2Ax_0\left(\frac{k_b}{k_a}\right) + \frac{A^2\left(k_b - k_a\right)}{2k_a^2} + \Delta, \tag{7}$$

$$W_{a\to b} = 2Ax_0 + A^2\left(\frac{1}{k_b} - \frac{1}{k_a}\right). \tag{8}$$

These equations can be combined to obtain an expression for the $|a\rangle \to |b\rangle$ efficiency $\eta_{a\to b}$

$$\eta_{a\to b} = \frac{2Ax_0 + A^2\left(\frac{1}{k_b} - \frac{1}{k_a}\right)}{2k_b x_0^2 + 2Ax_0\left(\frac{k_b}{k_a}\right) + \frac{A^2\left(k_b - k_a\right)}{2k_a^2} + \Delta}. \tag{9}$$

The maximum A that can be applied to the system is limited by the necessity that there exist two stable minima that the molecule can be switched between. In other words, the efficiency will be maximized at A_{stop} and this maximum efficiency is η_{stop}. Again, for $V = 0$, we calculate

$$A_{stop} = \left(\frac{k_b}{k_a - k_b}\right)\left[2k_a x_0 - k_b\sqrt{4k_a k_b x_0^2 - 2\Delta\left(k_b - k_a\right)}\right]. \tag{10}$$

Substituting this value back into Eq. (9) allows us to obtain a general expression for the efficiency at the stop force (η_{stop})

$$\eta_{stop} = \frac{2k_a k_b}{k_a^2 - k_b^2}\left|\frac{\Delta\left(k_b - k_a\right) - 2k_a k_b x_0^2 + k_a x_0\sqrt{4k_a k_b x_0^2 + 2\Delta\left(k_a - k_b\right)}}{2k_a k_b x_0^2 + \Delta\left(k_a - k_b\right)}\right|. \tag{11}$$

Note that this expression is valid for any value of Δ, positive or negative. In Fig. 4, we plot $\eta_{a\to b}$ as a function of A for $k_a/k_b = 1$. For this condition, $\eta_{a\to b}$ is an increasing function of A and is maximized at A_{stop} for all values of Δ. In fact, for the most common scenario where $\Delta \geq 0$, the efficiency is always maximized at A_{stop}. Only when $\Delta < 0$ and $k_a > k_b$ do, we find that the maximum $\eta_{a\to b}$ does not occur at A_{stop} but at an intermediate force. In this case, the maximum $\eta_{a\to b}$ can even surpass 1.0 (Supporting Information). For $\Delta < 0$, the large $\eta_{a\to b}$ values are an artifact of our neglect of the energetic cost of preparing this state but serve to illustrate how the 1D system can be "pre-loaded" to produce more mechanical energy than the input photon.

For the remainder of this paper, we will concentrate on the $\Delta \geq 0$ case that is most relevant for practical materials. Note that our model assumes that the quantum yield for isomerization is unity in all cases. The molecular parameters that determine efficiency are k_a, k_b, Δ, and V. To examine the role of the first three parameters in the limit of $V = 0$, in Fig. 5, we plot η_{stop} versus the ratio k_a/k_b for various Δ values. The first observation is that η_{stop} is maximized for $\Delta = 0$. For $\Delta > 0$, the efficiency decreases as the input energy cost increases, as predicted by Eq. (9). The behavior of η_{stop} as a function of the force constants is more complex. When $k_a = k_b = k$, Eq. (11) reduces to

$$\eta = \frac{2Ax_0}{2kx_0^2 + 2Ax_0 + \Delta}. \tag{12}$$

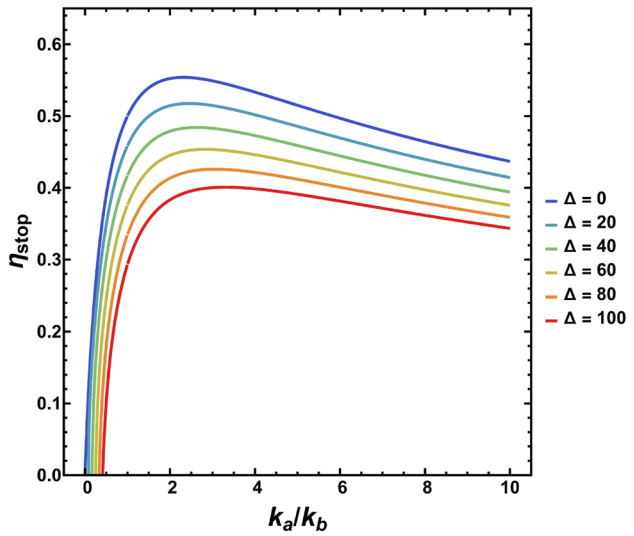

Fig. 5 The photomechanical efficiency η_{stop} plotted as a function of k_a/k_b for different values of Δ. When Δ > 0, smaller ratios of k_a/k_b become inaccessible (and thus $\eta = 0$) as only one stable minimum exists along under the absence of applied force

In this limit, $A_{stop} = kx_0 - \Delta/(2kx_0)$ and we find

$$\eta_{stop} = \frac{2kx_0^2 - \frac{\Delta}{k}}{4kx_0^2 + \Delta\left(1 - \frac{1}{k}\right)}. \tag{13}$$

This expression leads to a maximum $\eta_{stop} = 0.5$ when $\Delta = 0$. However, the largest η_{stop} values are obtained for $k_a/k_b > 1$ for all Δ values, meaning that the $|b\rangle$ PES has a lower frequency and a shallower well. We found a maximum efficiency η_{stop} of 0.554 for $k_a/k_b = 2.315$ and $\Delta = 0$. At larger Δ values, the maximum η_{stop} decreases and shifts to slightly larger k_a/k_b ratios; for example, a maximum occurs at $k_a/k_b = 3.307$ when $\Delta = 100$.

The origin of the higher η_{stop} values for $k_a/k_b > 1$ lies in the modified optical properties, rather than the increased force generation. The lower k_b value reduces the photon energy required to make the transition between $|a\rangle$ and $|b\rangle$ surfaces, as illustrated in Fig. 6a. The different dependences of Eqs. (7) and (8) on the force constants k_a and k_b mean that it is possible to dramatically reduce the cost of the $\Delta E_{a\to b}$ photon by lowering k_b while only slightly decreasing the work output. Once k_b is much smaller than k_a, however, both the work output and photon input energies decline at the same rate. This can be seen from a plot of the $W_{a\to b}$ and $\Delta E_{a\to b}$ values as a function of the k_a/k_b ratio, shown in Fig. 6b. The 10% gain in photon-to-work efficiency for $k_a > k_b$ provides a hint that the work output can be enhanced by tuning the molecular vibrational structure. Previous workers have established that vibrational structure and coherence near conical intersections can have a large impact the quantum yield of a photochemical reaction [26–28]. The results presented here assume that the photochemical quantum yield is unity, so the photon-to-work efficiency reflects how vibrational structure affects the light absorption process which occurs far from this type of intersection of the harmonic surfaces. In a real system, the effects of molecular vibrational structure on both the conical intersection and the absorption energy will both have to be considered to accurately calculate the overall photon-to-work efficiency.

If $V \neq 0$, the A_{stop} and η_{stop} values can be evaluated numerically by iteratively solving Eqs. (3), (10), and (11). Details are given in the Supporting Information. The effect of V on η_{stop} is shown in Fig. 7, which plots η_{stop} as a function of V for different values of Δ. In all cases, increasing V leads to a roughly linear decrease in η_{stop}. This can be understood as a consequence of the nonadiabatic coupling leading to a lowered activation barrier on the adiabatic ground state surface, which in turn lowers A_{stop}. At large V values, the second minimum at x_b disappears, preventing the calculation of η_{stop} values.

Finally, we consider the cycling efficiency of the 1D coupled harmonic system. We have already evaluated the efficiency in the $|a\rangle \to |b\rangle$ direction. The return $|b\rangle \to |a\rangle$ stroke does not contribute to the work against the applied force, but does require extra photon energy, so the efficiency will always be decreased. In this case, the overall efficiency of the $|a\rangle \to |b\rangle \to |a\rangle$ cycle is just

$$\eta_{cycle} = \frac{W_{a\to b}}{\Delta E_{a\to b} + \Delta E_{b\to a}}. \tag{14}$$

We consider the case of $\Delta \geq 0$, where the starting state $|a\rangle$ is the lowest energy isomer. At the maximum η_{stop}, the $|a\rangle$ PES curve intersects the minimum of the $|b\rangle$ PES curve, and the photon energy required to make the $|b\rangle \to |a\rangle$ transition becomes negligible. In this case, the maximum $\eta_{cycle} = \eta_{stop} = 0.554$ for $k_a/k_b = 2.315$. This analysis indicates that the highest cycle efficiency will be attained for T-type materials, since in practice, this return transition would be accomplished by thermal excitation rather than an optical photon. Lower A values not only lead to lower forward $|a\rangle \to |b\rangle$ efficiencies but also require additional input photon energy to return the system from $|b\rangle$ to $|a\rangle$.

3 Discussion

There are several reasons that the analysis presented above should be considered an upper limit for photomechanical efficiencies in real systems. First, we only considered the $T = 0$ K limit. When $\Delta E^{\ddagger} < kT$, we can expect thermal fluctuations to effectively remove the stationary point at the $|b\rangle$ curve minimum. In practice, this would lower A_{stop} and thus

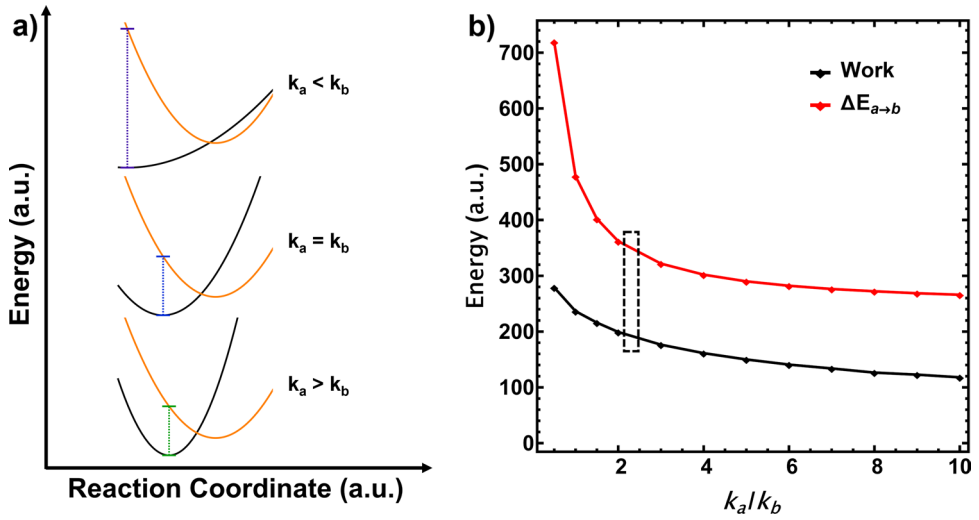

Fig. 6 **a** Illustration of how changes in k_a/k_b lead to different $\Delta E_{a\to b}$ energy gaps for $A = 5$. Both the energy cost and work output decrease as the k_a/k_b ratio increases, but at different rates, leading to the maximum in the efficiency seen in Fig. 5. **b** Plots of the available work (black) and photon cost $\Delta E_{a\to b}$ (red) as k_a/k_b increases for $x_0 = 11$, $V = 0$, and $\Delta = 0$. The photon cost asymptotically approaches 250 a.u. as k_a/k_b increases, while the work continues to decrease and reduces the one-way efficiency at higher ratios of k_a/k_b. The maximum efficiency occurs in the dashed region ($k_a/k_b = 2.315$) where the photon cost has decreased more rapidly than the work output

η_{stop}. Second, we have assumed that the photochemical quantum yield for the $|a\rangle \to |b\rangle$ reaction is unity. The efficiencies calculated above should be multiplied by a quantum yield factor that in practice is always less than 1.0 due to both radiative and nonradiative decay channels. Third, we have only considered a 1D system with coupled product-reactant modes. In a polyatomic molecule with many modes oriented orthogonal to the reaction coordinate, e.g., azobenzene [29–31], much of the input photon energy will be dissipated into vibrations that are not aligned with the applied force, further decreasing the efficiency.

How efficient could a molecular photoisomerization be in practice? Gaub and coworkers investigated the photomechanical response of single oligomer chains composed of azobenzene repeat units attached to an atomic force microscope tip. In these experiments, the applied force was not aligned with the *cis–trans* reaction coordinate, which is usually taken to be the C–N–N dihedral angle. Even given this misalignment, however, measurements of the chain contraction under load yielded an absorbed photon-to-work efficiency of 0.1 for a *trans* → *cis* photoisomerization [32]. This value is actually not far from the single-molecule theoretical limit derived in this paper. However, once quantum yields, absorption cross sections, and light propagation were taken into account, the calculated incident photon-to-work efficiency was estimated to be 7.5×10^{-6}. [33] Photomechanical crystals composed purely of photoactive molecules typically exhibit absorbed photon-to-work efficiencies of less than 1%. [34, 35], as do most polymer systems [36]. The large gap between the theoretical molecular limit and the measured efficiencies suggests that there remains a substantial room to improve these materials.

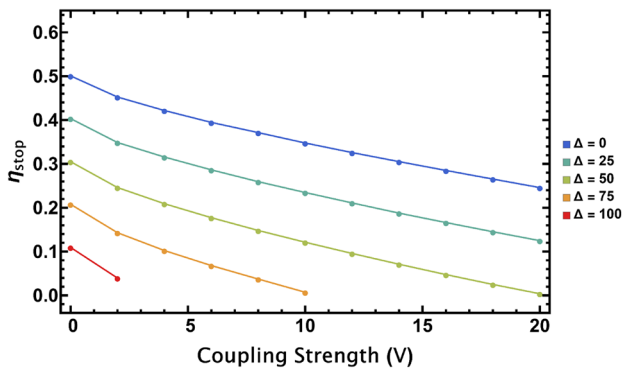

Fig. 7 The photomechanical efficiency η_{stop} is plotted as a function of the electronic coupling V for various Δ values. For these calculations, $x_0 = 5$ and $k_a = k_b = 1$. Note that larger V couplings and Δ values result in smaller Astop and, thus, η_{stop} values as the ground state barrier decreases

The results presented above suggest that directional application of force could result in changes in molecular optical properties. Although redshifts are commonly observed in high-pressure experiments, they usually result from changes in the medium polarizability due to increased density [37, 38]. When the molecular PESs are distorted by the application of a directional force, our model predicts a blueshift of the $|a\rangle \to |b\rangle$ absorption and a redshift of the $|b\rangle \to |a\rangle$ fluorescence. Although challenging, the measurement of optical properties during the directional pulling of single molecules could reveal the PES deformations illustrated in Fig. 2. If applying a force leads to substantial absorption shifts, then a fruitful area for improving photomechanical materials might

involve tuning of reactant–product vibrational structures to enhance efficiency. The fact that even in this simple model, the maximum efficiency does not occur for $k_a/k_b = 1.0$ suggests that careful consideration of how molecular vibrations affect both photon absorption and mechanical response properties may be necessary to optimize these materials.

Finally, we can compare molecular photomechanical elements to photovoltaic approaches for transforming photon energy into work. At 0 K and given an input photon at the semiconductor band edge, the photovoltaic energy conversion efficiency can approach 1.0 [39]. Piezoelectric actuators have a maximum electrical-to-mechanical conversion efficiency of 0.5 [40], so assuming no electrical losses, the PV-piezoelectric approach would yield an overall efficiency of $1.0 \times 0.5 = 0.5$. If the PV cell is attached to a DC electric motor, whose electrical-to-mechanical efficiency can approach 1.0 [41], then the photon-to-work efficiency will also approach 1.0. Our results show that the photomechanical approach can be competitive with either photovoltaic approach in terms of theoretical efficiency. The photomechanical approach possesses several potential advantages, however, including (1) simplicity, since only a single element with no connections is required; (2) insensitivity to electromagnetic fields, since no free carriers are generated; (3) fast response, since the molecular shape change follows the photoisomerization time, which can be on the order of picoseconds. For a given application, the best approach will likely be determined by factors like device size, environment, and the available light source. It should be emphasized that the field of photomechanical materials is still relatively young compared to the fields of electromagnetic actuators and photovoltaics, so considerable improvement may be expected.

4 Conclusion

The simple 1D model in this paper represents a preliminary step in the development of a molecular model for the photomechanical process. It provides a way to estimate mechanical outputs like the stop force, work, and efficiency from molecular parameters like vibrational frequencies, reaction coordinates, and electronic couplings. A central result is that the theoretical photon-to-work efficiency of a molecule is comparable to that of photovoltaic devices. A second result is that the maximum efficiency is obtained when $k_a > k_b$, showing that the interplay between force-induced changes in the optical as well as the mechanical properties must be considered in the design of such molecules. It is hoped that this work will motivate more sophisticated theoretical studies and materials design that enable bulk photomechanical systems to approach the molecular performance limits.

Supplementary Information The online version contains supplementary material available at https://doi.org/10.1007/s43630-022-00261-9.

Acknowledgements This work was supported by the Office of Naval Research through the MURI on Photomechanical Material Systems (ONR N00014-18-1-2624).

Declarations

Conflict of interest On behalf of all authors, the corresponding author states that there is no conflict of interest.

References

1. White, T. J. (2017). *Photomechanical Materials, Composites, and Systems* (1st ed.). Wiley.
2. Koshima, H. (2020). *Mechanically Responsive Materials for Soft Robotics*. Wiley.
3. Kuzyk, M. G., & Dawson, N. J. (2020). Photomechanical materials and applications: A tutorial. *Advanced Optics Photonics, 12*, 847–1011. https://doi.org/10.1364/AOP.387366
4. Han, B., Zhang, Y.-L., Chen, Q.-D., & Sun, H.-B. (2018). Carbon-based photothermal actuators. *Advanced Functional Materials*. https://doi.org/10.1002/adfm.201802235
5. Lui, B. F., & Bardeen, C. J. (2021). Using small molecule absorbers to create a photothermal wax motor. *Small (Weinheim an der Bergstrasse, Germany)*. https://doi.org/10.1002/smll.202105356
6. Hasebe, S., Hagiwara, Y., Komiya, J., Ryu, M., Fujisawa, H., Morikawa, J., Katayama, T., Yamanaka, D., Furube, A., Sato, H., Toru, A., & Koshima, H. (2021). Photothermally driven high-speed crystal actuation and its simulation. *Journal of the American Chemical Society, 143*, 8866–8877. https://doi.org/10.1021/jacs.1c03588
7. Kundys, B. (2015). Photostrictive materials. *Applied Physical Review, 2*, 011301. https://doi.org/10.1063/1.4905505
8. Kim, T., Zhu, L., Al-Kaysi, R. O., & Bardeen, C. J. (2014). Organic photomechanical materials. *ChemPhysChem, 15*, 400–414. https://doi.org/10.1002/cphc.201300906
9. Ikeda, T., Mamiya, J.-I., & Yu, Y. (2007). Photomechanics of liquid-crystalline elastomers and other polymers. *Angewandte Chemie International Edition, 46*, 506–528. https://doi.org/10.1002/anie.200602372
10. Priimagi, A., Barrett, C. J., & Shishido, A. (2014). Recent twists in photoactuation and photoalignment control. *Journal of Materials Chemistry C, 2*, 7155–7162. https://doi.org/10.1039/C4TC01236D
11. White, T. J. (2018). Photomechanical effects in liquid crystalline polymer networks and elastomers. *Journal of Polymer Science. Part B, 56*, 695–705. https://doi.org/10.1002/polb.24576
12. Al-Kaysi, R. O., Muller, A. M., & Bardeen, C. J. (2006). Photochemically driven shape changes of crystalline organic nanorods. *Journal of the American Chemical Society, 128*, 15938–15939.

13. Kobatake, S., Takami, S., Muto, H., Ishikawa, T., & Irie, M. (2007). Rapid and reversible shape changes of molecular crystals on photoirradiation. *Nature, 446*, 778–781.
14. Koshima, H., Ojima, N., & Uchimoto, H. (2009). Mechanical motion of azobenzene crystals upon photoirradiation. *Journal of the American Chemical Society, 131*, 6890–6891.
15. Bushuyev, O. S., Tomberg, A., Friscic, T., & Barrett, C. J. (2013). Shaping crystals with light: Crystal-to-crystal isomerization and photomechanical effect in fluorinated azobenzenes. *Journal of the American Chemical Society, 135*, 12556–12559.
16. Nath, N. K., Pejov, L. O., Nichols, S. M., Hu, C., Saleh, N. I., Kahr, B., & Naumov, P. E. (2014). Model for photoinduced bending of slender molecular crystals. *Journal of the American Chemical Society, 136*, 2757–2766. https://doi.org/10.1021/ja4101497
17. Wang, H., Chen, P., Wu, Z., Zhao, J., Sun, J., & Lu, R. (2017). Bending, curling, rolling, and salient behavior of molecular crystals driven by [2+2] cycloaddition of a styrylbenzoxazole derivative. *Angewandte Chemie International Edition, 56*, 9463–9467.
18. Durr, H., & Bouas-Laurent, H. (1990). *Photochromism: Molecules and Systems*. Elsevier.
19. Kitagawa, D., & Kobatake, S. (2016). Strategy for molecular design of photochromic diarylethenes having thermal functionality. *Chemical Record, 16*, 2005–2015. https://doi.org/10.1002/tcr.201600060
20. Bell, G. I. (1978). Models for the specific adhesion of cells to cells. *Science, 200*, 618–627. https://doi.org/10.1126/science.347575
21. Barbara, P. F., Meyer, T. J., & Ratner, M. A. (1996). Contemporary issues in electron transfer research. *Journal of Physical Chemistry, 100*, 13148–13168. https://doi.org/10.1021/jp9605663
22. Benderskii, V. A., Vetoshkin, E. V., Kats, E. I., & Trommsdorff, H. P. (2005). A semiclassical 1D model of ultrafast photoisomerization reactions. *Chemical Physics Letters, 409*, 240–244. https://doi.org/10.1016/j.cplett.2005.05.025
23. Beyer, M. K., & Clausen-Schaumann, H. (2005). Mechanochemistry: The mechanical activation of covalent bonds. *Chemical Reviews, 105*, 2921–2948. https://doi.org/10.1021/cr030697h
24. Evans, E., & Ritchie, K. (1997). Dynamic strength of molecular adhesion bonds. *Biophysical Journal, 72*, 1541–1555. https://doi.org/10.1016/S0006-3495(97)78802-7
25. Ribas-Arino, J., & Marx, D. (2012). Covalent mechanochemistry: Theoretical concepts and computational tools with applications to molecular nanomechanics. *Chemical Reviews, 112*, 5412–5487. https://doi.org/10.1021/cr200399q
26. Malhado, J. P., & Hynes, J. T. (2012). Photoisomerization for a model protonated Schiff base in solution: Sloped/peaked conical intersection perspective. *The Journal of Chemical Physics, 137*, 22A543. https://doi.org/10.1063/1.4754505
27. Levine, B. G., & Martınez, T. J. (2007). Isomerization through conical intersections. *Annual Review of Physical Chemistry, 58*, 613–634. https://doi.org/10.1146/annurev.physchem.57.032905.104612
28. Duan, H.-G., Miller, R. J. D., & Thorwart, M. (2016). Impact of vibrational coherence on the quantum yield at a conical intersection. *Journal of Physical Chemistry Letters, 7*, 3491–3496. https://doi.org/10.1021/acs.jpclett.6b01551
29. Yu, J. K., Bannwarth, C., Liang, R., Hohenstein, E. G., & Martínez, T. J. (2020). Nonadiabatic dynamics simulation of the wavelength-dependent photochemistry of azobenzene excited to the nπ* and ππ* excited states. *Journal of the American Chemical Society, 142*, 20680–20690. https://doi.org/10.1021/jacs.0c09056
30. Aleotti, F., Soprani, L., Nenov, A., Berardi, R., Arcioni, A., Zannoni, C., & Garavelli, M. (2019). Multidimensional potential energy surfaces resolved at the RASPT2 level for accurate photoinduced isomerization dynamics of azobenzene. *Journal of Chemical Theory and Computation, 15*, 6813–6823. https://doi.org/10.1021/acs.jctc.9b00561
31. Crecca, C. R., & Roitberg, A. E. (2006). Theoretical study of the isomerization mechanism of azobenzene and disubstituted azobenzene derivatives. *Journal of Physical Chemistry A, 110*, 8188–8203. https://doi.org/10.1021/jp057413c
32. Hugel, T., Holland, N. B., Cattani, A., Moroder, L., Seitz, M., & Gaub, H. E. (2002). Single-molecule optomechanical cycle. *Science, 296*, 1103–1106. https://doi.org/10.1126/science.1069856
33. Holland, N. B., Hugel, T., Neuert, G., Cattani-Scholz, A., Renner, C., Oesterhelt, D., Moroder, L., Seitz, M., & Gaub, H. E. (2003). Single molecule force spectroscopy of azobenzene polymers: Switching elasticity of single photochromic macromolecules. *Macromolecules, 36*, 2015–2023. https://doi.org/10.1021/ma021139s
34. Dong, X., Tong, F., Hanson, K. M., Al-Kaysi, R. O., Kitagawa, D., Kobatake, S., & Bardeen, C. J. (2019). Hybrid organic-inorganic photon powered actuators based on aligned diaryethene nanocrystals. *Chemistry of Materials, 31*, 1016–1022. https://doi.org/10.1021/acs.chemmater.8b04568
35. Halabia, J. M., Ahmeda, E., Sofelab, S., & Naumov, P. (2021). Performance of molecular crystals in conversion of light to mechanical work. *Proceedings of the National Academy Sciences of the United States of America, 118*, e2020604118. https://doi.org/10.1073/pnas.2020604118
36. Cheng, L., Torres, Y., Lee, K. M., McClung, A. J., Baur, J., White, T. J., & Oates, W. S. (2012). Photomechanical bending mechanics of polydomain azobenzene liquid crystal polymer network films. *Journal of Applied Physics, 112*, 013513. https://doi.org/10.1063/1.4729771
37. Okamoto, B. Y., & Drickamer, H. G. (1974). High pressure studies of solvent effects on anthracene spectra. *Proceedings of the National Academy Sciences of the United States of America, 71*, 4757–4759. https://doi.org/10.1073/pnas.71.12.4757
38. Robertson, W. W., & King, A. D. (1961). Calculation of pressure shifts of optical absorption spectra from solvent data. *The Journal of Chemical Physics, 34*, 1511–1515. https://doi.org/10.1063/1.1701037
39. Muller, M. F., Freunek, M., & Reindl, L. M. (2013). Maximum efficiencies of indoor photovoltaic devices. *IEEE Journal of Photovoltaics, 3*, 59–64. https://doi.org/10.1109/JPHOTOV.2012.2225023
40. Blackburn, J. F., & Cain, M. G. (2013). Coupling efficiency in piezoelectric actuators with direct current and alternating current excitation. *Journal of Applied Physics, 113*, 184101. https://doi.org/10.1063/1.4803480
41. Almeida, A. T. D., Ferreira, F. J. T. E., & Fong, J. A. C. (2011). Standards for efficiency of electric motors. *IEEE Industry Applications Magazine, 17*, 12–19. https://doi.org/10.1109/MIAS.2010.939427